doi.org/10.1002/cbdv.202300848 Research Article CHEMISTRY & BIODIVERSITY

www.cb.wiley.com

Analysis of Quinolinequinone Analogs with Promising Cytotoxic Activity against Breast Cancer

Ayse Mine Yilmaz Goler,[a] Ayse Tarbin Jannuzzi,[b] Abanish Biswas,[c] Subodh Mondal,[d] Vinay N. Basavanakatti,[e] Raghusrinivasan Jayaprakash Venkatesan,[f] Hatice Yıldırım,[g] Mahmut Yıldız,[h] Hülya Çelik Onar,[g] Nilüfer Bayrak,[i] Venkatesan Jayaprakash,[c] and Amaç Fatih TuYuN*[i]

It is quite challenging to find out bioactive molecules in the vast chemical universe. Quinone moiety is a unique structure with a variety of biological properties, particularly in the treatment of cancer. In an effort to develop potent and secure antiproliferative lead compounds, five quinolinequinones (**AQQ1-5**) described previously have been selected and submitted to the National Cancer Institute (NCI) of Bethesda to envisage their antiproliferative profile based on the NCI Developmental Therapeutics Program. According to the preliminary *in vitro* single-dose anticancer screening, four of five quinolinequinones (**AQQ2-5**) were selected for five-dose screening and they displayed promising antiproliferative effects against several cancer types. All AQQs showed a excellent anticancer profile with low micromolar GI_{50} and TGI values against all leukemia cell lines, some non-small cell lung and ovarian cancer, most colon, melanoma, and renal cancer, and in addition to some breast cancer cell lines. **AQQ2-5** reduced the proliferation of all leukemia cell lines at a single dose and five additional doses, as well as some non-small cell lung and ovarian cancer, the majority of colon cancer, melanoma and renal cancer, and some breast cancer cell lines. This motivated us to use *in vitro*, *in silico*, and *in vivo* technologies to further investigate their mode of action. We investigated the *in vitro* cytotoxic activities of the most promising compounds, **AQQ2** and **AQQ3**, in HCT-116 colon cancer, MCF7 and T-47D breast cancer, and DU-145 prostate cancer cell lines, and HaCaT human keratinocytes. Concomitantly, IC_{50} values of **AQQ2** and **AAQ3** against MCF7 and T-47D cell lines of breast cancer, DU-145 cell lines of prostate cancer, HCT-116 cell lines of colon cancer, and HaCaT human keratinocytes were determined. **AQQ2** exhibited anticancer activity through the induction of apoptosis and caused alterations in the cell cycle. *In silico* pharmacokinetic studies of all analogs have been carried out against ATR, CHK1, WEE1, CDK1, and CDK2. In addition to this, *in vitro* ADME and *in vivo* pharmacokinetic profiling for the most effective AAQ (**AAQ2**) have been studied.

1. Introduction

Cancer is known as a disease of the cells, which are the fundamental element of human organs and tissues, but it can affect almost any part of the body. The human body consists of billions of cells. While old cells die, the others generate new cells by dividing them into two. Albeit all cancers differ from each other, every cancer starts with an increase of abnormal cells. The production of new cells is repeated millions of times a day in the body. Some cells that become abnormal in the body do behave differently from normal cells, such as living longer or growing and dividing faster. In the progress of time, the abnormal cells form cancer by multiplying out of control. Cancer could spread into tissues and nearby lymph nodes with the lapse of time. This process might happen by moving through the blood or lymphatic systems.[1] What we know about cancer treatments is mainly based on stopping or slowing down the development and spread of cancer that

[a] *A. M. Yilmaz Goler*
Department of Biochemistry, School of Medicine/Genetic and Metabolic Diseases Research and Investigation Center, Marmara University, 34854 İstanbul, Türkiye

[b] *A. Tarbin Jannuzzi*
Department of Pharmaceutical Toxicology, Faculty of Pharmacy, İstanbul University, 34116 İstanbul, Türkiye

[c] *A. Biswas, V. Jayaprakash*
Department of Pharmaceutical Sciences & Technology, Birla Institute of Technology, Mesra, 835215 Ranchi, Jharkhand, India

[d] *S. Mondal*
Bioanalysis, Eurofins Advinus BioPharma Services India Pvt Ltd., 560058 Bengaluru, India

[e] *V. N. Basavanakatti*
Adgyl Lifesciences Private Limited, 560058 Bengaluru, India

[f] *R. Jayaprakash Venkatesan*
Department of Industrial and Systems Engineering, Faculty of Interdisciplinary Sciences & Engineering, Indian Institute of Technology, 721302 Kharagpur, India

[g] *H. Yıldırım, H. Çelik Onar*
Department of Chemistry, Engineering Faculty, Istanbul University-Cerrahpasa, Avcilar, 34320, İstanbul, Türkiye

[h] *M. Yıldız*
Department of Chemistry, Gebze Technical University, Gebze, 41400 Kocaeli, Türkiye

[i] *N. Bayrak, A. F. TuYuN*
Department of Chemistry, Faculty of Science, Istanbul University, Fatih, 34126 İstanbul, Türkiye
E-mail: aftuyun@gmail.com
aftuyun@istanbul.edu.tr

works by removing abnormal cells, killing them, or stopping them from growing and dividing. One of the main cancer treatments is chemotherapy. Besides, the drugs used in this treatment are not considered adequate, mainly because of low efficacy and undesirable side effects, highlighting the urgency to find out effective and safe drugs.[2] Numerous successful compounds and natural product analogs have been identified as a consequence of numerous efforts to create and find secure and effective therapeutic candidates.[3,4] *In silico* studies are applied to improve molecules with greater potential efficacy to combat the undesirable toxicological effects by concentrating on physicochemical properties.[5] Furthermore, the investigation of the structure–activity relationship (SAR) has given crucial information on how structural alterations may increase potency and bioavailability in the development of safe new therapeutics.[6]

Over the last decades, the generation of 1,4-quinones has received considerable attention due to their various biological activities such as antibacterial,[7,8] antifungal,[9,10] anticancer,[11,12] antiHIV,[13] antimalarial,[14,15] antiplatelet,[16,17] antiallergic,[17] anti-infective,[18] anti-inflammatory,[19] antithrombotic,[20,21] lipoxygenase inhibitory,[22] and human monoamine oxidase (MOA) inhibitory.[23] Quinone moiety also makes up the main motif of some well-known drugs that are either clinically approved or that are currently in various phases of clinical and preclinical development,[24,25] such as idebenone, streptonigrin, cribrostatin 5, mitomycin C, mitoxantrone, doxorubicin, and daunorubicin. The drug idebenone, produced by Takeda Pharmaceutical Company Ltd., is used to treat emotional disorders linked to cerebrovascular illnesses.[26] Streptonigrin, a substance derived from *Streptomyces flocculus* cultures,[27,28] has a wide variety of biological activity against several cancer cell lines, including those from the breast, melanoma, and lung.[29] Additionally, further studies on doxorubicin[30] have shown that it is a chemotherapy drug and is used for the treatment of many different types of cancer by slowing or stopping the growth of cancer cells in the blockage of an enzyme called topoisomerase II.[31] There are some reports related to mitoxantrone in metastatic breast cancer and acute myeloid leukemia.[32,33]

The review, recently published by Dahlem Junior et al.,[34] suggests that quinone-based compounds could be used in antimicrobial or antitumoral applications as an efficient molecular scaffold. Quinones containing the amino (aryl amino, piperidino, or piperazino groups), sulfanyl[35] or alkoxy group[36,37] were investigated and proved to be potent agents for therapeutic candidates. Within these libraries, aminoquinones are the prominent structures because of their ability to effectively fine-tune physicochemical and pharmacokinetic properties. Hence, the combination of amines and 1,4-quinones simply leads to conceptually attractive and effective aminoquinones. As an example, Li et al. reported aminoquinones containing naphthoquinone unit incorporated with S3I–201 derivatives which are known as effective STAT3 inhibitors.[38] A set of quinone-based compounds were prepared by Morris et al. for their colorectal cancer profile against 293T, HCT-116, and SW480 cell lines and two of obtained molecules have a potential to inhibit the Wnt/β-catenin signaling pathway *via* inhibition of the TCF4/DNA interaction.[39]

In our previous studies, our group has introduced to the literature the aminated and/or thiolated lead structures as anticancer and/or antibacterial agents based on 1,4-quinone scaffolds, also named as Plastoquinone and quinolinequinone analogs.[40–44] Encouraged by all these good results and in continuation of our studies on the generation of new lead structures, we herein undertake to carry out extensive studies aiming at the identification of new lead molecules for the treatment of cancer. Five target quinolinequinones containing electron-withdrawing groups were synthesized and submitted to the National Cancer Institute of Bethesda within the Developmental Therapeutics Program[45] with the protocol of the Drug Evaluation Branch, NCI[46] to be tested at a single-dose concentration of 10 μM on nine different cancer types including leukemia, lung, colon, CNS, melanoma, ovarian, renal, prostate, and breast cancer cell lines.[47] Following single-dose evaluation, the DTP division of the NCI chose four of five quinolinequinones (**AQQ2-5**) for a complete panel five-dose *in vitro* experiment to determine their GI_{50} on the sixty cell lines. Based on by the NCI results, two quinolinequinones (**AQQ2** and **AQQ3**) were investigated for cytotoxicity against the HCT-116, DU-145, MCF7, and T-47D cell lines. Additionally, we made the decision to look into how the chosen quinolinequinones (**AQQ2** and **AQQ3**) affected breast cancer by cell cycle distribution, apoptosis and necrosis rate, and the generation of reactive oxygen species (ROS) analyses. Thorough *in silico* docking simulations including protein-ligand interactions and ADME properties along with *in vivo* studies were also carried out to learn more about the host-guest interactions of powerful quinolinequinones.

2. Methods and Materials

2.1. Biological Evaluation

2.1.1. In vitro Single-Dose Anticancer Screening by NCI

The obtained quinolinequinones were submitted to National Cancer Institute (NCI), Bethesda, USA and as per standard protocol of NCI, all compounds were evaluated for their antiproliferative activity at single-dose assay (10 μM concentration in DMSO) on a panel of 60 cancer cell lines derived from leukemia, non-small cell lung, colon, CNS, melanoma, ovarian, renal, prostate, and breast as per protocol. Tested compounds were added to the microtiter culture plates followed by incubation for 48 h at 37 °C. Sulforhodamine B (SRB), a protein-binding dye, was used for endpoint determination. The percent of the growth of the treated cells was determined in comparison to the untreated control cells and the results of each tested compound were reported. Data from one-dose experiments pertain to the percentage growth at 10 μM.[47–49]

2.1.2. In vitro Five-Dose Anticancer Screening by NCI

Serial 5×10-fold dilution from an initial DMSO stock solution was performed, prior to incubation at each individual concentration. The most promising quinolinequinones (**AQQ2**, **AQQ3**, **AQQ4**, and **AQQ5**) were then elevated by DTP-NCI for a higher testing level to determine three dose-response parameters (GI_{50}, TGI, and LC_{50}) for each cell lines after establishing a dose-response curve from 5 different concentrations 0.01, 0.1, 1, 10, and 100 μM for **AQQ2**, **AQQ3**, **AQQ4**, and **AQQ5**. The exact detailed procedure for the latter assay had been elaborated earlier.

The GI_{50} is the concentration of test drug where 100×(T−T0)/(C−T0) = 50. Herein, T explains the optical density of the test well after a 48 h period of treatment with test drug, T0 explains the optical density at time zero ultimately C is the control optical density. The "50" is called the GI50PRCNT, a T/C-like parameter that can have values from +100 to −100. The TGI is the concentration of test drug where 100×(T−T0)/(C−T0) = 0. The LC_{50} is the concentration of drug where 100×(T−T0)/T0 = −50.

2.1.3. Cell culture and treatments

HCT-116 colon cancer, T-47D breast cancer, DU-145 prostate cancer cells, and HaCaT human keratinocytes were cultured in DMEM with L-glutamine and MCF7 breast cancer cells were cultured in DMEM/F12 with L-glutamine and both supplemented with 10% fetal bovine serum and 1×antibiotic/antimicotic solution (ThermoFisher Gibco, MA, USA). The cells were maintained in a humidified 5% CO_2 atmosphere and subcultured routinely when reached 80% confluence.

2.1.4. Cytotoxic evaluation with 3-(4,5-dimethylthiazol-2-yl)-2,5-diphenyltetrazolium bromide (MTT) assay

To determine the cytotoxic potential of the **AQQ2** and **AQQ3**, the cells were seeded at a seeding density of 1×10^4/well in 96-well plates and incubated overnight. The different concentrations of **AQQ2** and **AQQ3** (1, 2.5, 5, 10, 25, 50 and 100 μM) were added to the culture medium and incubated for 24 h. ADRI was used as positive control drug at the same concentrations. Then, MTT solution was added to the wells and incubated for a further 3h. After removing the supernatant, the formazan salt dissolved with DMSO and the absorbance was measured at 590 nm using BioTek Epoc plate reader. The inhibitory concentration 50 (IC_{50}) values of the compounds were calculated with GraphPad Prism 7.

2.1.5. Apoptotic cell evaluation

Fluorochrome labeled Annexin V and PI was used to detect necrotic, apoptotic and live cells (FITC Annexin V Apoptosis Detection with PI, SONY Biotechnology, USA). Cells were plated at 1×10^6 cell/well density in 6-well plate. Following incubation with 1, 2.5, and 5 μM **AQQ2** and 2.5 μM ADRI for 24 h, cells were trypisinized, and resuspended in 500 μL of 1×Binding Buffer. 3 μL PI and 5 μL Annexin V-FITC were added to the cells at room temperature and incubated for 15 min in a dark place. After incubation cells were analyzed by flow cytometry (FACS Calibur, Becton Dickinson, USA.) Upper left (UP), upper right (UR), lower right (LR), and lower left (LL) dials are available. Necrotic cells are observed in the UL quadrant and are stained with PI. Cells labeled with PI + Annexin V in the UR quadrant indicate the proportion of cells in late apoptosis. The ratio of cells in the early apoptotic stage is calculated using annexin-stained cells in the LR channel. The cells in the LL quadrant were dubbed live cells since they were not stained with any dye. The percentage of the apoptotic and necrotic cells were calculated using BD CellQuest Pro Software (Becton Dickinson, USA).

2.1.6. Oxidative stress evaluation with DCFH-DA assay

MCF7 cells were plated in 6-well plates at a density of $1x10^6$ cells/well. After overnight incubation, the cells were treated with 1, 2.5 and 5 μM **AQQ2** for 24 h. As a positive control, the cells were treated with 100 μM H_2O_2 for 30 mins. After incubation, the cells were collected by trypsinization and stained with 20 μ DCFH-DA for 15 mins at dark. Then, the cells were washed with PBS and quantified with BD FACS Calibur flow cytometry.

2.1.7 Cell cycle assay

Cells were treated with **AQQ2** and ADRI as described before the apoptotic evaluation for cell cycle assay. For cell cycle analysis, 1×10^6 cells were harvested, followed by centrifugation, and the supernatant was discarded. The remaining pellet was suspended in PBS and 70% cold ethanol. Finally, the cells were washed once with PBS followed by incubation in PBS containing 50 mg/mL PI and 2 mg/mL DNase-free RNase-A for 30 mins at room temperature in the dark and then analyzed by BD FACS Calibur Flow Cytometry System (Becton Dickinson, USA). Cell percentages belonging to the phases of the cell cycle were determined by software in comparison with the control group.

2.1.8. Statistical analysis

The results were expressed as the mean ± SD of three biological replicates. The statistical comparisons were done with one-way ANOVA followed by the Tukey test or two-way ANOVA followed by the Dunnett test. All data were analyzed using Prism V.7.04 (GraphPad Software). Statistical significance was set at $P < 0.05$.

2.2. In silico Studies

2.2.1. ADME

We used ADMETlab 2.0 to evaluate the ADMET properties, physicochemical properties, and medicinal chemistry friendliness of the chemical compound under investigation. ADMETlab 2.0 is a web-based platform that utilizes predictive models and algorithms to comprehensively evaluate the ADMET properties of chemical compounds. We input the SMILES notation of the compound into the ADMETlab 2.0 interface and used the available modules to obtain information on permeability, bioavailability, plasma protein binding, distribution volume, and fraction unbound. We also analyzed the compound's toxicity profile using ADMETlab 2.0's toxicity prediction modules. The resulting data were analyzed and interpreted to gain insights into the compound's ADMET properties which were compared with *in vitro* data.

2.2.2. Molecular Docking

Experimental XRD 3D-structure of selected target proteins retrieved from the Protein Data Bank (PDB). Missing residues were constructed, and proteins were prepared for docking using Modeler and Dockprep module implemented in UCSF Chimera. Autodock parameter files (protein.gpf and ligand.dpf) were prepared using python utility scripts from MGLTools-1.5.7. Docking simulation was carried out in Google Colab using GPU enabled virtual machine. AutoDock-GPU was used to run the molecular docking simulation with 300 runs for each ligand. For interaction analysis lowest energy conformer from the largest cluster was considered. Python utility scripts from MGLTools-1.5.7 was used to pick the lowest energy conformer from the largest cluster and to prepare the complex.pdb files for interaction analysis using LigPlot+.

2.3. In vivo Pharmacokinetic Study

2.3.1. In vitro metabolic stability study

Liver microsomes of mouse (Cat. No. M1000, Lot. No. 1710069), rat (Sprague-Dawley, male, Cat. No. R1000, Lot. No. 1610290), dog (Beagle, male, Cat. No. D1000, Lot. No. 1310086) and human (Cat. No. H0610, Lot. No. 1610016) of Xeno Tech LLC, Kansas, USA were used for testing the metabolic stability of **AQQ2**. A final protein (liver microsomal) concentration of 0.5 mg/mL and final test substance (**AQQ2**) concentration of 0.5 μM were used for the study. To the respective microsomes at a volume of 12.5 μL in the well, 2.5 μL of **AQQ2** (100 uM in acetonitrile: dimethyl sulfoxide, 96:4) in the presence and absence of NADPH (50 μL, 10 mM) were added and the final volume made up to 500 μL with sodium phosphate buffer (50 mM, pH 7.4). The one without NADPH served as control. Sampling (50 μL) were done at the following time points: 0, 5, 10, 15, and 30 min for sample and at 0 and 30 min for control. Acetonitrile (150 μL) was used as quenching solvent, internal standard (Rolipram) was added, vortexed/centrifuged and the aliquot from the supernatant was analyzed using LC-MS/MS. All the experiments were performed in duplicate.

2.3.2. In vivo Bioavailability Study of AQQ2 in Male Sprague-Dawley Rats

Experimentation on animals were approved by the Institutional Animal Ethics Committee and were conducted as per the guidelines of Committee for the Purpose of Control and Supervision of Experiments on Animals (CPCSEA), Ministry of Social Justice and Environment, Government of India. Sprague-Dawley rats (HyLasco Biotechnology (India) Pvt. Ltd., a subsidiary of Charles River from US) of 8–12 weeks, weighing between 220 and 320 g were housed in poly sulfonate cages. They were maintained at 25±3 °C temperature 50–70% of relative humidity with approximately 12 h light and dark cycle. Before, during and after the study period the animals were having access to rat maintenance diet (Altromin Spezialfutter, GmbH, Germany) and purified water (UV-treated, charcoal filtered). Rats selected for study were cannulated in Jugular vein, and prior to dosing (except IV dose) were kept under fasting overnight. Post-dosing, access to food and water offered after a gap of ~4 h. For IV administration at a dose level of 1 mg/kg bw (10 mL/kg), AQQ2 was prepared in NMP (10%)+PBS (pH 7.4) qs. For PO administration at a dose of 5 mg/kg bw (10 mL/kg), **AQQ2** was formulated in NMP (10%)+Cremophor EL (5%)+PEG400 (30%)+PG (20%)+PBS (pH 7.4) qs. Dosing volumes were calculated based on the weight of animal weight on the day of dosing and were administered accordingly. Blood samples (~0.250 mL) were collected after dosing from the jugular vein at following time points: 0.083 (IV only), 0.25, 0.5, 1, 2, 4, 6, 8, and 24 h adopting serial sampling design (heparinized saline was used to maintain the volume following each sample collection). Pre-labelled microcentrifuge tubes containing K_2EDTA (20 μL of 200 mM solution per mL of blood) as anticoagulant were used for collecting the blood samples and were then stored at −60 °C until bioanalysis using fit-for-purpose LC/MS/MS method. Pharmacokinetic parameters were calculated using non-compartmental analysis (NCA) tool of the validated Phoenix® WinNonlin® 8.3.

2.3.3. Bioanalytical Method (LC/MS/MS) for AQQ2

2.3.3.1. Chemicals and reagents

MS grade (≥99.0% pure) ammonium formate and formic acid were sourced from Sigma Aldrich. HPLC grade acetonitrile (ACN) and dimethyl sulfoxide solvents were purchased from Merck Germany. Milli-Q® Water used for the preparation of mobile phase, rinsing solvent and seal washes was obtained from the inhouse (Eurofins Advinus limited) Milli-Q® system. The internal standard MQD04 ($C_{17}H_{13}ClN_2O_3$, 328.74, purity of ≥97%) used in the study was procured from Sigma Aldrich. A

SCIEX API 4000™ LC/MS/MS triple quadrupole mass spectrometer system equipped with a negative Electrospray ionization (ESI) source and Shimadzu prominence HPLC comprising of binary pumps, column oven and SIL-HTC autosampler was used in the study. Data acquisition, integration and quantification were performed using Analyst® 1.6.3.

2.3.3.2. Chromatographic and Mass Spectrometric Conditions

Liquid chromatographic separations of **AQQ2** and internal standard, MQD04, were achieved on a reverse phase Synergi Fusion RP 50×4.6 mm, 5 µm column operating at 40 °C. The gradient mobile phase was used starting with an initial 90:10, 3 mins: 10:90, 6 mins: 10:90, 6.10 mins: 90:10 up to 8 min. 5 mM ammonium formate with 0.1% formic acid (Mobile phase A) and 0.1% formic acid in Acetonitrile (Mobile phase B) delivered at a flow rate of 0.6 mL/min without splitter. Mass spectrometer was operated in negative electrospray ionization mode with unit mass resolution in a quadrupole analyzer with 200 ms dwell time and the analytes were detected by multiple reaction monitoring (MRM). The compound parameters of **AQQ2** and MQD04 (internal standard) were optimized along with the MRM transition (*m/z*) to achieve sensitivity. Source parameters were optimized to a curtain gas N_2 flow of 25 psi (CUR), nebulizer N_2 gas of 40 psi (gas 1), ion spray voltage of +5500 V (IS), auxiliary N_2 gas of 60 psi (gas 2) with turbo spray temperature of 450 °C (TEMP) and collision-activated dissociation gas (CAD) of 10 psi. MRM transition (*m/z*) selected for the analyte **AQQ2** was 367.10/332.20, 367.10/304.20 and 367.10/197.20 and MQD04 (Internal standard) was 330.20/299.30. System suitability test was performed prior to analysis of samples. System suitability test comprised of six replicate injections of extracted ULOQ and an extracted blank and LLOQ sample from rat plasma. The percentage coefficient of variation (CV (%)) for peak area ratio (analyte to internal standard) of six replicate injections was ≤5%, which met the acceptance criteria. The retention time was within ±0.5 min variation in each analytical run.

Sample Preparation: Extraction of **AQQ2** and MQD04 (Internal standard) from samples of rat plasma has been done by a protein precipitation (crashing) method. To 50 µL of CC/QC/Study samples, 200 µL of Internal Standard Working Solution in acetonitrile was added to all the tubes except for Standard Blank sample, vortexed to mix. Vortexed (Vibramax 100, Heidolph Instruments) for about 10 min. Centrifuge (Eppendorf 5810R) the above samples for 10 min at 10000 rpm at a set temperature of 4 °C. Aliquot sufficient volume of supernatant into auto-sampler vials for analysis in LC/MS/MS (SCIEX API 4000).

2.3.3.3. Preparation of calibration standards and quality control samples

The stock solutions of **AQQ2** and MQD04 (internal standard) were prepared in Dimethyl sulfoxide (DMSO) and acetonitrile, respectively at 1 mg/mL concentration. The stock solution of **AQQ2** was further diluted using DMSO to prepare calibration standard solutions in the concentration range of 22 to 25000 ng/mL. For internal standard, acetonitrile was used to prepare a working solution of concentration 500 ng/mL. These solutions were then spiked in interference-free rat blank plasma to obtain calibration standards in the pharmacologically relevant range (1.1 to 1250 ng/mL). Similarly, the quality control (QC) samples were prepared using independent stock solutions of analytes to obtain the concentrations of 3.00, 500 and 1000 ng/mL in rat plasma, representing low, medium and high concentration QC samples, respectively. The stock solutions, diluted standard solutions, quality control solutions and internal standard solution were stored at 2–8 °C. The spiked plasma samples (calibration standards and quality controls) were prepared freshly prior to sample analysis.

3. Results and Discussions

3.1. Biological Results

3.1.1. Preliminary in vitro Single-Dose Anticancer Screening

Herein, the previously synthesized aminated quinolinequinones (**AQQ1-5**) containing electron-withdrawing group(s) shown in Figure 1 were evaluated for their *in vitro* activity against cancer cell lines by the NCI.[50] The data were summarized as the growth percentage (GP) and lethality (values less than 0) of the treated cells in Table 1. All the aminated quinolinequinones (**AQQ1-5**) having a trifluoromethyl or cyano group in a different position on arylamine moiety were totally inactive and/or weak active against most of the cancer cell lines such as non-small cell lung cancer, CNS cancer, melanoma (except that MALME-3M and M14), ovarian cancer (except that IGROV1 and OVCAR-3), renal cancer (except that UO-31), prostate cancer, and breast cancer (except that MCF7 and T-47D). Moderate activities were observed against COLO 205 (colon cancer, with 83.32 inhibition), MALME-3M (melanoma, with 72.99 inhibition), M14 (melanoma, with 71.36 inhibition), IGROV1 (ovarian cancer, with 72.18 inhibition), UO-31 (renal cancer, with 83.75 inhibition), and MCF7 (breast cancer, with 81.25 inhibition) cell lines. On the other hand, there is a good correlation between our previous studies[51–53] about the anticancer activity against some leukemia cancer cell lines. Looking specifically at four AQQ analogs, **AQQ4** and **AQQ5** displayed promising anticancer activity against the sub-panel cell lines of leukemia. Interestingly, the **AQQ3** displayed maximum sensitivity towards HCT-116 (colon cancer cell lines) with 98.58% inhibition in tumor cell growth. Whereas **AQQ4** displayed potency against HCT-15 (98.11% inhibition) the colon cancer cell lines, OVCAR-3 (95.76% inhibition) of the ovarian cancer cell lines, UO-31 (83.75% inhibition) of the renal cancer cell lines, MCF7 and T-47D (81.25% and 92.02% inhibition) of the breast cancer cell lines, **AQQ5** showed biological activity against HCT-15 and SW-620 (93.18% and 97.59% inhibition) of the colon cancer cell lines, IGROV1 (72.18% inhibition) of the ovarian cancer cell

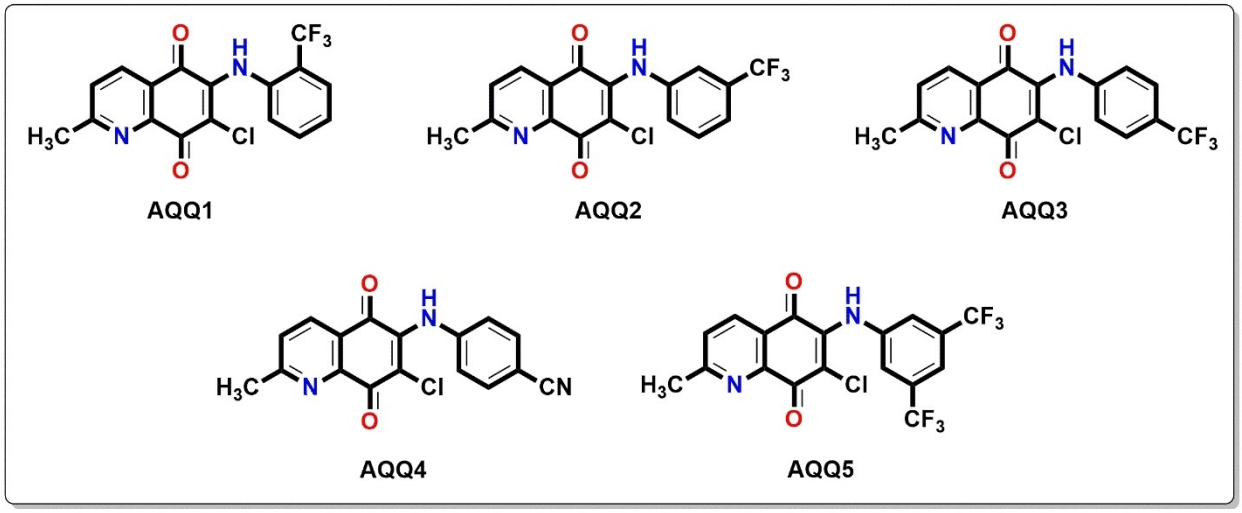

Figure 1. The structures of the aminated quinolinequinones (**AQQ1**–**5**) containing electron-withdrawing group(s) in different positions involved in the current exploration.

lines, and UO-31 (90.29% inhibition) of the renal cancer cell lines.

3.1.2. In vitro Full Panel Five-Dose 60-Cell Line Assay

Showing promising results satisfying the threshold inhibitory criterion in the single-dose assay from NCI, four quinolinequinones (**AQQ2**, **AQQ3**, **AQQ4**, and **AQQ5**) were selected as the lead analogs for further investigation against a panel of 60 human cancer cell lines at a five-dose screening at 10-fold dilutions in the range of 0.01–100 μM. For the purpose of determining the tested quinolinequinones' biological potential, three response parameters (GI50, TGI, and LC50) were utilized. TGI represents total growth inhibition, whereas GI_{50} indicates the concentration at which 50% of growth inhibitory action is present. The LC_{50} value represents the concentration at which 50% of cancer cells death.[47,48] In Tables 2–4, three response parameters for sub-panel cell lines are shown: GI_{50}, TGI, and LC_{50} (all in μM).

As seen in Tables 2–4, the selected four quinolinequinones (**AQQ2**, **AQQ3**, **AQQ4**, and **AQQ5**) exhibited remarkable broad-spectrum anticancer activity against all leukemia cell lines not only with GI_{50} values in the range 0.291–2.23 μM, but also with TGI values in the range 1.05–6.08 μM. Aside from the HL-60(TB) cell lines, all of the leukemia cell lines in the panel had LC_{50} values more than 100 μM. **AQQ2** was found to be highly sensitive against non-small cell lung cancer EKVX (GI_{50} = 1.90 μM), HOP-92 (GI_{50} = 1.91 μM), and NCI–H23 (GI_{50} = 1.82 μM); colon cancer COLO 205 (GI_{50} = 1.82 μM), HCT-116 (GI_{50} = 1.51 μM), and HCT-15 (GI_{50} = 1.66 μM); most of the cell lines of melanoma in the range of 1.51–1.95 μM; ovarian cancer IGROV1 (GI_{50} = 1.87 μM), OVCAR-3 (GI_{50} = 1.68 μM), and OVCAR-4 (GI_{50} = 1.56 μM); most of the cell lines of renal cancer in the range of 1.54–1.80 μM; prostate cancer DU-145 (GI_{50} = 1.80 μM); most of the cell lines of breast cancer in the range of 1.77–1.93 μM. **AQQ2** also showed superior cytotoxic activity against some or all cell lines of non-small cell lung, colon, melanoma, ovarian, renal, prostate, and breast cancer with TGI not more than 10 μM. Last but not least, **AQQ2** demonstrated strong fatal activity against the majority of cell lines with the exception of non-small cell lung cancer (NCI–H226, NCI–H23, and NCI–H522), colon, melanoma, ovarian, renal, prostate, and breast cancer (MCF7, MDA-MB-231/ATCC, and T-47D) cell lines. Figure 2 shows the five-dose response curves for the **AQQ2** for the whole panel of 60 human cancer cell lines. Additionally, **AQQ3** displayed high activity with GI_{50} values ranging from 0.291–2.00 μM against some of the tested cancer cell lines. A remarkable activity was recorded against non-small cell lung EKVX, HOP-92, NCI–H226, NCI–H23, and NCI–H522; colon cancer HCT-116, HCT-15, and SW-620; melanoma LOX IMVI, M14, and UACC-257; ovarian cancer IGROV1, OVCAR-3, and OVCAR-4; renal cancer 786–0, ACHN, CAKI-1, RXF 393, and UO-31; prostate cancer DU-145; all breast cancer cell lines (except that HS 578T). Also, this quinolinequinone (**AQQ3**) possessed significant TGI values ranging from 2.02–5.03 μM against most of the tested cancer cell lines. Related to LC_{50}, some of none-small cell lung cancer cell lines (NCI–H226 and NCI–H522), colon cancer cell lines (SW-620), ovarian cancer cell lines (OVCAR-4), and as well as breast cancer cell lines (MCF7 and T-47D) displayed values exceeding 100 μM. Finally, the last two quinolinequinones (**AQQ4** and **AQQ5**) demonstrated outstanding anticancer activity against three non-small cell lung cancer cell lines (HOP-92, NCI–H23, and NCI–H522) with GI_{50} values ranging from 1.57 to 1.95 μM, in addition to their TGI values ranged from 3.41 to 5.97 μM against the mentioned cell lines. Their LC_{50} values ranged from 6.78 to over 100 μM. Other important results for **AQQ4** were obtained with colon cancer COLO 205, HCT-116, HCT-15, and SW-620 (1.66, 1.83, 1.74, and 1.76 μM, respectively); melanoma LOX IMVI, MALME-3M, and UACC-257 (1.53, 1.74, and 1.64 μM, respectively); ovarian cancer OVCAR-3 and OVCAR-4 (1.84 and 1.59 μM, respectively); renal

Table 1. Anticancer activity results as per single-dose assay at 10 μM concentration as percent cell growth of the aminated quinolinequinones (**AQQ1**–**5**).

Cell line	AQQ1	AQQ2	AQQ3	AQQ4	AQQ5
CCRF-CEM	61.74	4.32	2.47	3.83	4.75
HL-60(TB)	50.62	32.26	35.81	17.44	40.71
K-562	70.12	3.08	7.13	5.72	4.18
MOLT-4	75.36	6.52	8.71	7.64	9.31
RPMI-8226	85.95	-17.61	-8.81	55.05	6.65
SR	89.85	9.01	10.5	15.29	7.46
A549/ATCC	106.67	104.69	101.99	106.12	100.78
EKVX	91.53	58.06	77.21	92.96	78.0
HOP-62	101.81	141.33	97.18	115.37	117.58
HOP-92	95.86	107.33	71.3	125.83	92.37
NCI-H226	97.77	73.27	89.46	98.28	84.3
NCI-H23	92.09	52.3	68.53	92.26	85.95
NCI-H322M	99.79	107.97	106.97	108.71	105.18
NCI-H460	100.85	101.28	100.73	100.44	95.92
NCI-H522	94.27	-28.75	-18.76	52.38	37.44
COLO 205	105.79	105.57	16.68	79.58	92.49
HCC-2998	116.92	108.13	97.87	107.79	96.52
HCT-116	99.95	-25.91	1.42	67.92	41.96
HCT-15	89.68	-61.12	-58.6	1.89	6.82
HT29	109.84	105.31	96.83	106.3	101.64
KM12	99.79	106.13	98.21	102.06	97.02
SW-620	85.76	-0.81	-10.47	-23.12	2.41
SF-268	90.18	100.18	97.71	96.96	87.05
SF-295	104.04	109.62	112.14	118.02	95.74
SF-539	92.51	106.02	100.67	100.4	93.95
SNB-19	105.11	101.15	97.49	96.37	90.59
SNB-75	90.1	109.4	115.31	109.58	98.28
U251	100.76	95.67	91.46	96.62	85.16
LOX IMVI	97.59	-61.83	-57.06	70.39	66.22
MALME-3M	101.72	-5.42	-49.61	27.01	47.9
M14	97.79	80.44	28.64	86.22	89.86
MDA-MB-435	103.59	71.34	95.78	99.48	93.76
SK-MEL-2	100.86	99.65	103.11	103.72	74.46
SK-MEL-28	101.83	78.5	51.03	99.76	88.66
SK-MEL-5	100.22	96.91	95.29	98.94	77.04
UACC-257	100.06	-4.17	35.56	74.83	75.24
UACC-62	94.92	97.57	96.61	95.72	79.87
IGROV1	78.35	-57.38	-58.24	68.35	27.82
OVCAR-3	66.64	-86.31	-48.55	4.24	37.27
OVCAR-4	64.1	-97.76	-96.42	-98.46	-84.85
OVCAR-5	102.67	118.52	109.51	106.28	109.35
OVCAR-8	101.59	76.03	39.27	91.5	87.82
NCI/ADR-RES	96.1	93.33	87.56	98.0	99.67
SK-OV-3	114.18	89.81	82.24	105.67	110.48
786-0	101.97	85.8	33.97	80.44	80.3
A498	75.39	86.02	79.04	61.62	80.35
ACHN	100.36	-96.16	-98.41	-58.53	-64.92
CAKI-1	97.66	81.78	44.37	76.46	81.39
RXF 393	104.49	-1.18	-15.72	92.09	74.53
SN12C	96.68	85.82	91.76	97.97	92.09
TK-10	128.88	126.87	85.36	103.86	105.82
UO-31	91.63	-67.65	-85.24	16.25	9.71
PC-3	81.84	69.56	72.4	89.56	80.53
DU-145	106.87	98.65	105.47	111.62	95.34
MCF7	85.78	-54.73	-56.15	18.75	-24.85
MDA-MB-231/ATCC	86.8	54.66	76.39	92.3	87.12
HS 578T	99.36	116.33	94.13	97.69	92.77
BT-549	144.15	122.98	129.74	119.92	114.65
T-47D	86.04	-41.86	-25.49	7.98	-9.18
MDA-MB-468	91.42	-65.16	-48.46	51.42	32.48

Table 2. GI_{50} values (in μM) of anticancer activity data as per at five-dose assay of the selected quinolinequinones (**AQQ2**, **AQQ3**, **AQQ4**, and **AQQ5**) after 48 h based on SRB assay at NCI (Values 100 refers to >100 and 0 refers to ND).

Cell line	AQQ2	AQQ3	AQQ4	AQQ5
CCRF-CEM	1.46	0.879	0.358	0.651
HL-60(TB)	1.5	1.4	1.08	0.547
K-562	0.31	0.291	0.351	0.412
MOLT-4	1.69	0.347	0.47	0.305
RPMI-8226	1.92	2.23	2.19	1.58
SR	1.56	0.367	0.375	0.31
A549/ATCC	20.1	100.0	35.6	16.9
EKVX	1.9	1.68	2.19	2.22
HOP-62	17.0	100.0	17.9	15.9
HOP-92	1.91	1.49	1.71	1.57
NCI-H226	2.57	1.89	4.36	5.36
NCI-H23	1.82	2.02	1.84	1.92
NCI-H322M	16.1	100.0	31.8	15.5
NCI-H460	18.4	100.0	30.2	13.7
NCI-H522	2.03	2.0	1.75	1.95
COLO 205	1.82	2.21	1.66	1.93
HCC-2998	2.6	3.14	3.83	4.61
HCT-116	1.51	0.569	1.83	1.43
HCT-15	1.66	1.36	1.74	1.83
HT29	2.6	2.81	3.06	2.39
KM12	15.9	70.3	19.9	12.3
SW-620	2.05	1.13	1.76	2.29
SF-268	4.76	3.57	8.36	6.38
SF-295	16.3	100.0	17.6	12.6
SF-539	3.18	1.92	10.2	5.4
SNB-19	16.0	11.6	15.7	13.8
SNB-75	13.0	100.0	6.79	9.23
U251	6.45	4.93	13.0	10.3
LOX IMVI	1.51	1.22	1.53	1.6
MALME-3M	1.79	1.9	1.74	1.67
M14	1.92	1.74	6.12	4.24
MDA-MB-435	1.95	2.12	6.99	4.67
SK-MEL-2	2.38	7.2	11.6	3.96
SK-MEL-28	1.95	2.06	2.46	2.21
SK-MEL-5	2.75	6.03	4.75	3.28
UACC-257	1.65	1.7	1.64	1.68
UACC-62	4.28	2.74	10.1	4.97
IGROV1	1.87	1.82	10.7	3.6
OVCAR-3	1.68	1.61	1.84	1.61
OVCAR-4	1.56	1.69	1.59	1.44
OVCAR-5	6.03	5.07	17.7	19.4
OVCAR-8	2.68	3.26	10.1	4.16
NCI/ADR-RES	2.65	2.62	3.55	2.74
SK-OV-3	14.2	100.0	11.7	13.9
786-0	1.8	1.84	1.74	1.72
A498	13.8	40.2	16.3	8.72
ACHN	1.78	1.82	1.81	1.92
CAKI-1	1.58	1.53	1.7	1.5
RXF 393	1.61	1.57	1.45	1.46
SN12C	2.16	2.31	5.68	4.55
TK-10	2.01	2.27	1.83	1.88
UO-31	1.54	1.37	1.54	1.41
PC-3	2.9	3.7	10.0	5.29
DU-145	1.8	1.87	2.13	2.6
MCF7	1.85	1.95	1.9	2.13
MDA-MB-231/ATCC	1.81	1.84	5.59	3.54
HS 578T	15.1	5.46	14.6	10.6
BT-549	2.16	1.78	2.79	1.86
T-47D	1.93	1.55	1.87	1.63
MDA-MB-468	1.77	1.89	1.78	2.01

cancer 786–0, ACHN, CAKI-1, RXF 393, TK-10, and UO-31 (1.74, 1.81, 1.70, 1.45, 1.83, and 1.54 μM, respectively); breast cancer MCF7, T-47D, and MDA-MB-468 (1.90, 1.87, and 1.78 μM, respectively). Concerning the TGI values of **AQQ4**, it showed superior activity with TGI in around 3 μM. Diminished lethality (more than 100 μM for LC_{50} values) was noticed with two breast

Table 3. TGI values (in μM) of anticancer activity data as per at five-dose assay of the selected quinolinequinones (**AQQ2**, **AQQ3**, **AQQ4**, and **AQQ5**) after 48 h based on SRB assay at NCI (Values 100 refers to >100 and 0 refers to ND).

Cell line	AQQ2	AQQ3	AQQ4	AQQ5
CCRF-CEM	4.71	3.89	2.2	3.59
HL-60(TB)	3.68	3.76	3.05	2.58
K-562	1.3	2.23	1.87	0.0
MOLT-4	5.37	2.99	2.56	1.05
RPMI-8226	5.91	6.08	5.74	5.14
SR	5.0	2.37	2.25	1.98
A549/ATCC	50.0	100.0	100.0	38.0
EKVX	4.24	3.98	5.59	5.45
HOP-62	31.8	100.0	50.7	31.3
HOP-92	3.89	3.19	3.41	3.52
NCI-H226	11.5	4.71	17.6	41.5
NCI-H23	4.67	5.59	4.58	4.94
NCI-H322M	30.3	100.0	100.0	31.8
NCI-H460	40.8	100.0	100.0	36.8
NCI-H522	5.12	4.93	3.75	5.97
COLO 205	3.78	4.83	3.51	4.31
HCC-2998	6.49	9.98	16.1	18.2
HCT-116	3.22	2.02	3.78	2.94
HCT-15	3.55	3.13	3.66	4.07
HT29	6.63	7.43	10.6	6.18
KM12	32.3	100.0	100.0	28.9
SW-620	4.89	3.73	3.87	5.32
SF-268	19.6	16.5	25.6	23.5
SF-295	31.2	100.0	39.2	25.8
SF-539	10.3	3.95	23.0	18.3
SNB-19	45.3	100.0	39.8	40.1
SNB-75	27.4	100.0	34.5	22.6
U251	24.8	20.5	28.7	23.5
LOX IMVI	3.33	3.04	3.46	3.49
MALME-3M	3.61	3.78	3.36	3.58
M14	4.39	3.36	21.9	17.9
MDA-MB-435	3.91	4.49	22.7	16.4
SK-MEL-2	5.73	32.8	24.6	15.6
SK-MEL-28	3.66	3.85	5.74	4.29
SK-MEL-5	7.84	21.2	17.3	11.4
UACC-257	3.24	3.27	3.17	3.3
UACC-62	18.4	10.7	25.9	19.3
IGROV1	3.6	4.04	24.7	14.1
OVCAR-3	3.11	3.03	3.51	3.02
OVCAR-4	3.27	4.31	3.08	2.79
OVCAR-5	22.1	19.8	34.8	38.4
OVCAR-8	8.93	100.0	28.2	24.2
NCI/ADR-RES	7.88	8.06	17.7	8.6
SK-OV-3	27.6	100.0	27.7	27.1
786-0	3.55	3.7	3.24	3.36
A498	27.9	100.0	100.0	22.0
ACHN	3.31	3.42	3.3	3.42
CAKI-1	3.01	3.01	3.31	2.94
RXF 393	3.0	2.95	2.79	2.82
SN12C	5.66	6.51	25.4	100.0
TK-10	3.52	3.75	3.27	3.31
UO-31	2.95	2.75	2.97	2.83
PC-3	11.5	20.7	25.1	20.0
DU-145	3.31	3.41	4.48	6.47
MCF7	4.66	5.03	4.62	5.45
MDA-MB-231/ATCC	4.01	4.63	25.8	14.0
HS 578T	85.6	59.7	56.1	76.4
BT-549	5.47	3.33	12.0	6.61
T-47D	4.8	5.06	4.79	5.18
MDA-MB-468	3.66	4.0	3.81	4.57

Table 4. LC_{50} values (in μM) of anticancer activity data as per at five-dose assay of the selected quinolinequinones (**AQQ2**, **AQQ3**, **AQQ4**, and **AQQ5**) after 48 h based on SRB assay at NCI (Values 100 refers to >100 and 0 refers to ND).

Cell line	AQQ2	AQQ3	AQQ4	AQQ5
CCRF-CEM	100.0	100.0	100.0	100.0
HL-60(TB)	9.02	11.8	8.6	100.0
K-562	100.0	100.0	100.0	100.0
MOLT-4	100.0	100.0	100.0	100.0
RPMI-8226	100.0	100.0	100.0	100.0
SR	100.0	100.0	100.0	100.0
A549/ATCC	100.0	100.0	100.0	85.1
EKVX	0.0	9.44	28.5	100.0
HOP-62	59.4	100.0	100.0	62.0
HOP-92	7.94	6.84	6.78	7.87
NCI-H226	100.0	100.0	55.9	100.0
NCI-H23	100.0	100.0	20.5	35.7
NCI-H322M	57.1	100.0	100.0	65.2
NCI-H460	90.2	100.0	100.0	98.4
NCI-H522	100.0	100.0	8.02	100.0
COLO 205	7.87	21.9	7.43	9.61
HCC-2998	25.7	40.8	50.0	55.1
HCT-116	6.9	5.24	7.82	6.06
HCT-15	7.58	7.21	7.69	0.0
HT29	100.0	100.0	77.6	100.0
KM12	65.8	100.0	100.0	68.4
SW-620	100.0	100.0	8.51	57.4
SF-268	64.5	73.3	70.6	68.9
SF-295	59.9	100.0	87.2	52.9
SF-539	38.2	8.14	51.9	45.6
SNB-19	100.0	100.0	100.0	100.0
SNB-75	57.5	100.0	100.0	51.7
U251	77.8	66.9	63.4	53.5
LOX IMVI	7.31	7.57	7.84	7.64
MALME-3M	7.28	7.49	6.49	7.68
M14	10.4	6.52	62.0	50.1
MDA-MB-435	7.85	9.49	61.5	42.6
SK-MEL-2	20.4	100.0	52.3	40.8
SK-MEL-28	6.87	7.18	20.1	8.35
SK-MEL-5	30.8	60.3	45.3	4.03
UACC-257	6.37	6.29	6.14	6.5
UACC-62	58.3	40.4	66.0	51.1
IGROV1	6.92	9.0	56.9	58.7
OVCAR-3	5.76	5.73	6.72	5.65
OVCAR-4	6.87	100.0	5.99	5.41
OVCAR-5	69.6	68.7	68.7	75.9
OVCAR-8	100.0	100.0	78.5	100.0
NCI/ADR-RES	100.0	100.0	100.0	100.0
SK-OV-3	53.8	100.0	65.5	52.8
786-0	7.01	7.43	6.04	6.55
A498	56.3	100.0	100.0	50.6
ACHN	6.14	6.44	6.01	6.12
CAKI-1	5.73	5.93	6.42	5.77
RXF 393	5.6	5.53	5.37	5.45
SN12C	100.0	100.0	96.3	100.0
TK-10	6.16	6.19	5.86	5.84
UO-31	5.64	5.49	5.71	5.69
PC-3	54.0	100.0	63.1	54.8
DU-145	6.09	6.19	9.44	25.0
MCF7	100.0	100.0	100.0	100.0
MDA-MB-231/ATCC	0.0	26.4	97.1	86.5
HS 578T	100.0	100.0	100.0	100.0
BT-549	19.8	6.22	36.1	26.6
T-47D	100.0	100.0	100.0	100.0
MDA-MB-468	7.57	8.43	8.19	100.0

cancer cell lines (MCF7 and T-47D). **AQQ5** displayed pronounced cytotoxicity with colon cancer COLO 205, HCT-116, and HCT-15 (1.93, 1.43, and 1.83 μM, respectively); melanoma LOX IMVI, MALME-3M, and UACC-257 (1.60, 1.67, and 1.68 μM, respectively); ovarian cancer OVCAR-3 and OVCAR-4 (1.61 and 1.44 μM, respectively); renal cancer 786–0, ACHN, CAKI-1, RXF

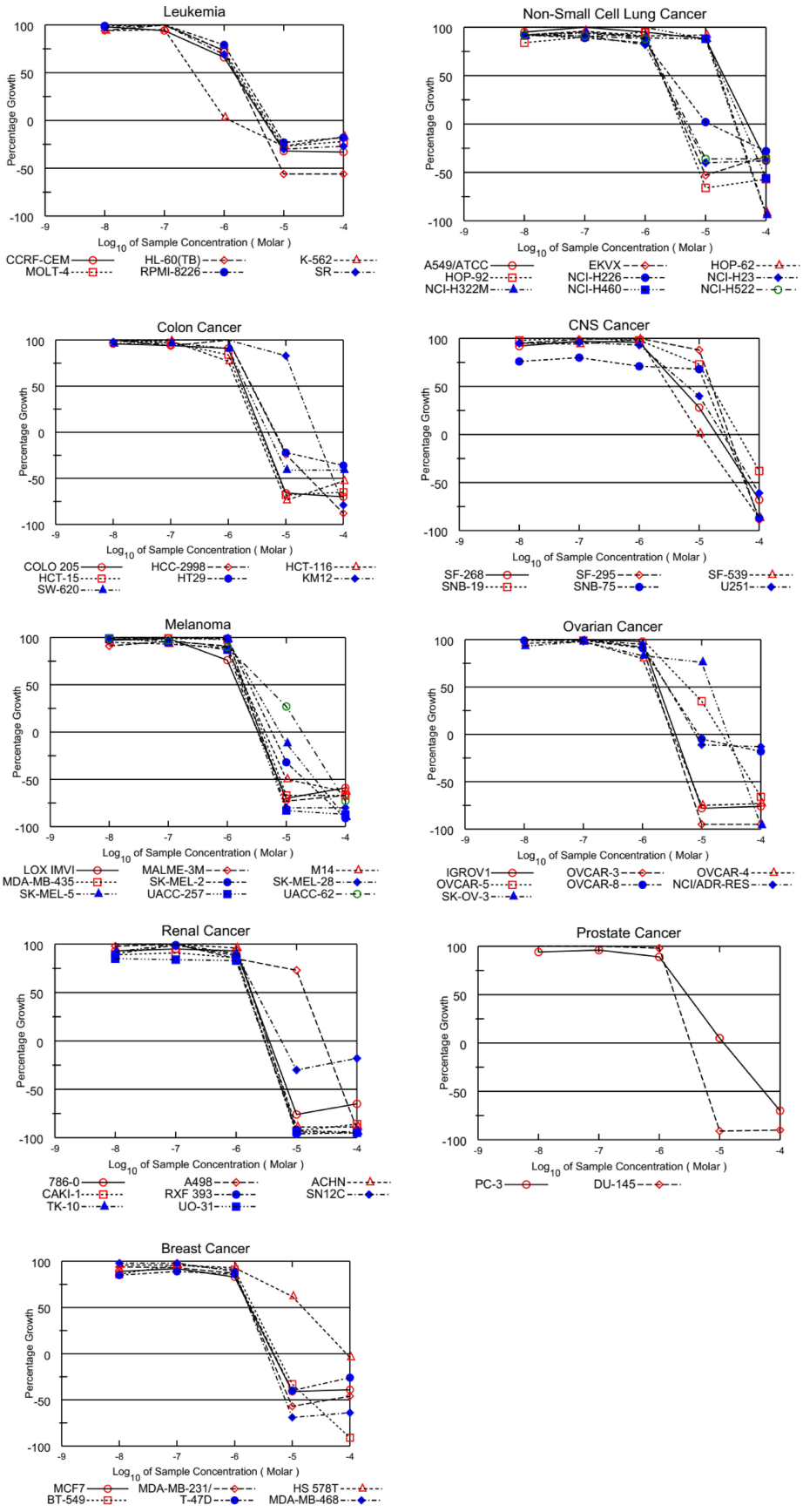

Figure 2. Graphical presentation of growth inhibition of the **AQQ2** at five-dose concentrations.

393, TK-10, and UO-31 (1.72, 1.92, 1.50, 1.46, 1.88, and 1.41 μM, respectively); breast cancer BT-549 and T-47D (1.86 and 1.63 μM, respectively). Besides, it exhibited remarkable TGI values more than 10 μM against the mentioned cancer cell lines. With regard to the lethality, it displayed LC_{50} values were found below 30 μM against the mentioned cancer cell lines except that T-47D.

3.1.3. Cytotoxic Evaluation of AQQ2 and AQQ3

From the NCI work compounds that contained $-CF_3$ electron-withdrawing groups at the *meta* and *para* positions (**AQQ2** and **AQQ3**) were selected for further *in vitro* evaluation. According to the NCI preliminary screening, we decided to use HCT-116 colon cancer, MCF7 and T-47D breast cancer, and DU-145 prostate cancer cells for evaluation. Also to determine the anticancer specificity of the compounds, we used HaCaT human keratinocytes. Each compound was tested with independent control group, and then administered at 1, 2.5, 5, 10, 25, 50, and 100 μM concentrations for each compound while creating graphs. **AQQ2** was not applied to the control group in Figure 3, it was defined as 0 μM. 0.1% DMSO is utilized as the cell and **AQQ2** solvent in the control media. Adriamycin (ADRI) was employed as a positive control in cell assays because it is a well-known treatment agent used in breast cancer therapy, and IC_{50} values were determined in MCF7 cells using the MTT protocol. According to the MTT results after 24 h treatment with **AQQ2** and **AQQ3**, we determined that **AQQ2** and **AQQ3** have the highest activity against MCF7 breast cancer cells with IC_{50} values of 1.63 ± 1.21 μM and 1.88 ± 1.56 μM, respectively. IC_{50} of the positive control drug, ADRI was 20.37 ± 5.21 μM as shown in Table 5. Also, when we checked the cytotoxicity of **AQQ2** and **AQQ3** against a non-cancerous cell lines, HaCaT, we determined IC_{50} values of 4.13 ± 1.14 μM and 3.63 ± 0.88 μM, respectively which were more than 2-fold higher than IC_{50} of MCF7 cell lines. This draws attention to the specificity of **AQQ2** and **AQQ3** against the MCF7 cell lines. According to the obtained cytotoxicity values, the molecules showed the second highest cytotoxic activity to T-47D cells followed by DU-145, and the weakest activity was observed against HCT-116 cells. Importantly, all of the IC_{50} values for studied cancer cell lines were lower than the IC_{50} values of ADRI and ADRI caused cytotoxicity against HaCaT cells at much lower doses than cancer cells (Figure 3). Thus, the specific anticancer activity of these compounds encouraged us to study further their mechanism of action. According to Table 5, the **AQQ2** compound examined the lowest IC_{50} values on MCF7 cells. Furthermore, these value were approximately three fold more effective on cancer cells (MCF7) than noncancerous cells

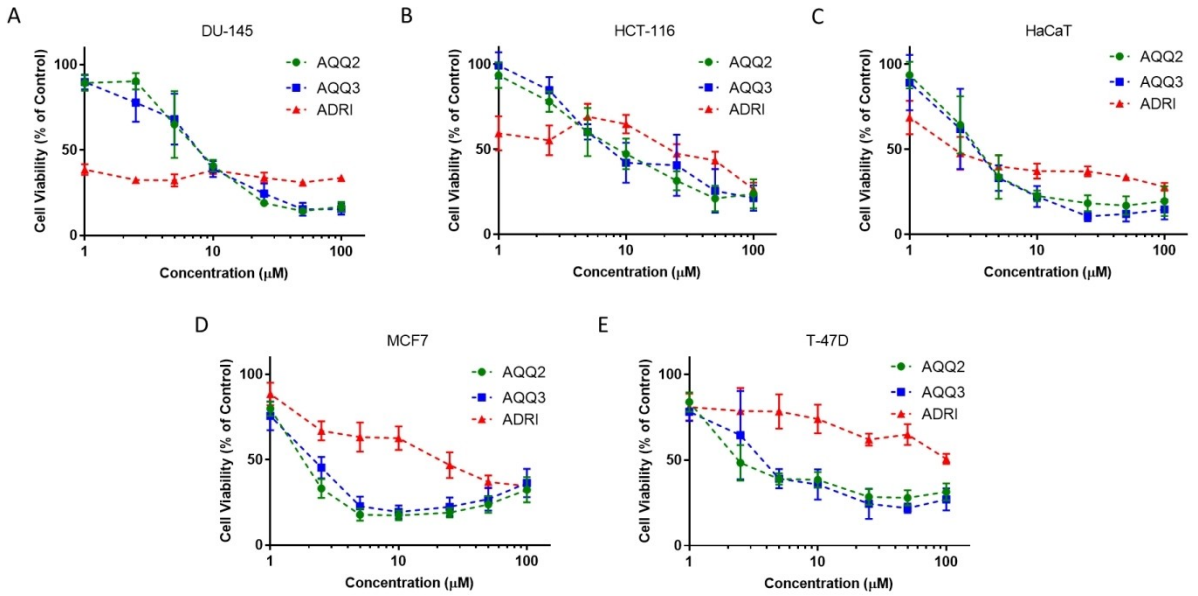

Figure 3. Cytotoxicity evaluation of 1–100 μM **AQQ2** and **AQQ3** treatments in DU-145 prostate cancer line (A), HCT-116 colon cancer (B), HaCaT human keratinocytes (C), MCF7 (D), and T-47D breast cancer (E) with MTT assay after 24 h treatment. Graphs in viability analysis with red triangles show cells treated with different concentrations of ADRI, blue squares show viability values for compounds **AQQ3**, while green circles show viability values for **AQQ2**.

Table 5. IC_{50} concentrations were calculated with MTT assay after 24 h of **AQQ2**, **AQQ3**, and **ADRI** treatments in HCT-116 colon cancer, MCF7 and T-47D breast cancer, DU-145 prostate cancer cells, and HaCaT human keratinocytes. The values are expressed as the mean ± SD.

(μM)	HCT-116	MCF7	T-47D	DU-145	HaCaT
AQQ2	10.44 ± 2.35	1.63 ± 1.21	4.627 ± 1.96	8.69 ± 1.59	4.13 ± 1.14
AQQ3	12.14 ± 3.58	1.88 ± 1.56	4.86 ± 1.95	8.51 ± 1.63	3.63 ± 0.88
ADRI	16.56 ± 9.24	20.37 ± 5.21	< 100	< 100	3.34 ± 1.55

(HaCaT). **AQQ2** showed slightly better anticancer activity and specificity than **AQQ3** and thus we continued our *in vitro* studies with **AQQ2**. Fluorine-containing quinone compounds were examined in a study similar to ours, which was recently published.[54] As a result of computation and *in vitro* analyses one hydroxybenzoquinone derivate was found to be more lethal on melanoma (A375) cells than vemurafenib (reference drug) and it has lower cytotoxic effects on fibroblast cells which indicates good cancer selectivity.[54]

3.1.4. Apoptotic and Necrotic Effects of AQQ2

Our group and other groups showed before apoptotic cell death induction with different quinolinequinone derivates in different cancer cells.[55,56] We want to determine the apoptotic effects of **AQQ2** in MCF7 cells. Flow cytometric analysis of apoptosis and necrosis showed that the apoptotic cell population increased with 2.5 μM **AQQ2** while the live cell population reduced significantly (Figure 4). The necrotic cell population did not show any change with **AQQ2** treatments. Also, the positive control drug ADRI caused a significant increase in the apoptotic cell population. According to our results, early apoptotic value of the 25 μM **AQQ2** applied groups was found to be significantly higher than control group, this result indicates that **AQQ2** can show its anticancer activity through apoptosis induction.

3.1.5. Effects of AQQ2 on Oxidative Stress

Physiological levels of ROS can be beneficial to cells by facilitating cell survival and proliferation. However, many chemotherapeutics show their cytotoxic activity by inducing oxidative stress drastically.[57] Thus, we tested whether **AQQ2** cytotoxicity is related to ROS production and we found that **AQQ2** significantly causes induction in the ROS levels in MCF7 cells (Figure 5). It was observed that the amount of ROS increased significantly compared to the control group, after the administration of 1 and 2.5 μM **AQQ2** to MCF7 cells.

3.1.6. Effects of AQQ2 on Cell Cycle Progression

Inhibition of cell cycle checkpoint function causes cell cycle arrest and can be effective in anticancer therapy.[58] A study showed that another quinolinequinone derivate, 6-anilino-5,8-quinolinequinone (LY83583), causes cell cycle inhibition in HCT-116 colorectal cancer cells.[59] To test cell cycle disruption potential of **AQQ2**, we analyzed cell cycle distribution by flow cytometry. Only low-dose **AQQ2** caused a significant decrease in G0/G1 cell population and these cells were distributed between S and G2/M phases (Figure 6). This indicates that **AQQ2** induced S and G2/M phase cell cycle arrest in MCF7 cells and this effect may contribute to its good anticancer activity against MCF7 cells. However, it is worth noting that this effect was not consistent with increasing doses of **AQQ2**.

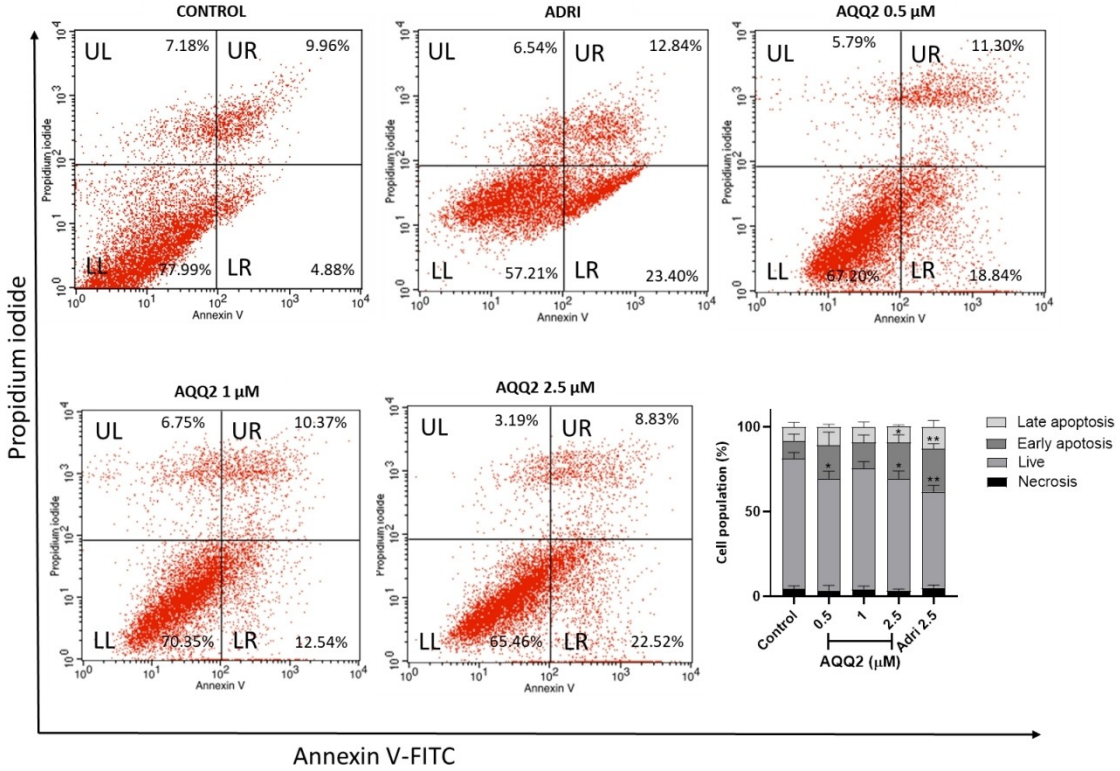

Figure 4. Flow cytometric analysis of apoptosis/necrosis rate in MCF7 cells after 24 h **AQQ2** treatment. Quadrant plots are shown for representative images and quantitative results. Quadrant statistics were used to study groups; each analysis recorded 10000 events. The bar graphs are shown the group values are expressed as mean ± SD (* $p < 0.05$, ** $p < 0.01$).

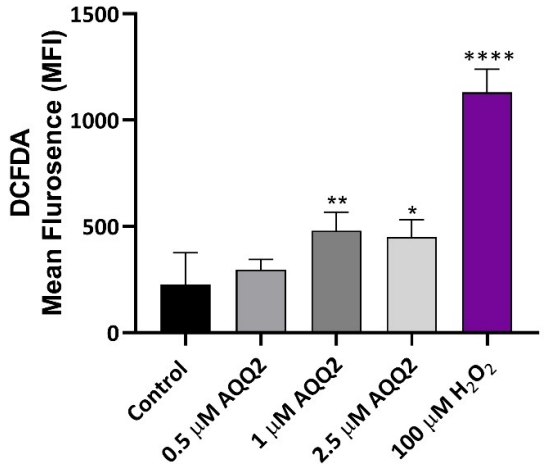

Figure 5. Flow cytometric analysis of ROS level in MCF7 cells after 24 h **AQQ2** treatment. The bar graph show the quantitative results of ROS production. The values as mean ± SD. (* $p < 0.05$, ** $p < 0.01$, **** $p < 0.0001$).

3.2. *In vitro* ADME and *in vivo* Pharmacokinetic Profiling

AQQ2 has not violated Lipinski's Ro5 as well as GSK rule. With LogP and LogD value of 2.03, **AQQ2** has significant lipophilicity in comparison with Veerapamil and Atenolol (relatively hydrophilic) ensuring better permeation profile across biological membranes to reach the site of action. Further, **AQQ2** has been subjected to *in vitro* ADME profiling (as shown in Table 6) and *in vivo* PK profiling. However, during the latter, the compound was not detectable in rat plasma samples due to anomalous profiles near the lowest calibration range. While there is no evidence of compound degradation under *ex vivo* conditions, it is believed that **AQQ2** may undergo rapid *in vivo* metabolism. The *in vitro* metabolic stability study, which employed rat liver microsomes, revealed that the drug was 100% metabolized within 30 min with a half-life of 4.0 min and a CL_{int} of 334.5 μL/min/mg protein. This may be the reason why we were unable to get the *in vivo* PK data for **AQQ2** in rat. Moreover, the evaluation with mouse, rat, dog and human liver microsomes was significantly high, ranging between 58.5 and 100%, indicating extensive first-pass metabolism in comparison with Verapamil. Extensive metabolism leading to increased clearance (CL_{int} 243.5–143740 μL/min/mg of protein) and shorter half-life (0.0–6.0 min) in the case of mouse, rat and human. Additionally, we predicted permeability through ADMETLab2.0 (https://admetmesh.scbdd.com/). Both Caco-2 (−4.699) and MDCK (1.8×10^{-5}) models predicted poor permeability and oral bioavailability ((F20% & F30%, -−)). Based on the *in vitro* and *in silico* data, a targeted delivery of the compound to the tumor environment may prove useful. Furthermore, a lead optimization strategy is being considered to improve the compound's permeability and metabolic stability through chemical modification of **AQQ2**.

3.3. Molecular Docking Simulation

Molecular docking simulation has been carried out to identify the putative target for these compounds (**AQQ1-5**). We considered three factors for selecting the probable target for this series of compounds. Firstly, the Molinspiration Server (https://www.molinspiration.com/cgi-bin/properties) predicted these compounds as kinase inhibitors with the score of 0.24. Secondly, compound **AQQ2** has been found to arrest the cell

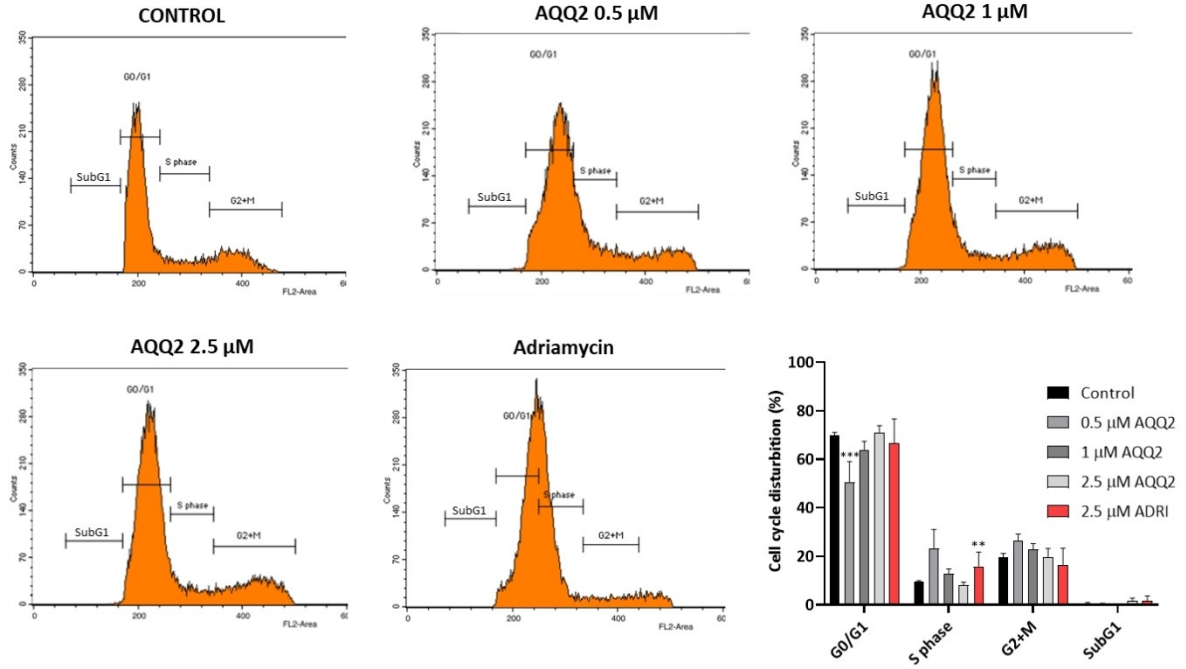

Figure 6. Flow cytometric analysis of cell cycle in MCF7 cells after 24 h **AQQ2** treatment. Representative cell cycle phase distribution histograms in four stages; Sub-G_1, G_0/G_1, S and G_2+M phase, and the quantitative result of cell cycle analysis. The values are expressed as the mean ± SD. (** $p < 0.01$, *** $p < 0{,}001$).

Table 6. *In vitro* ADME profiling of compound **AQQ2**.

		AQQ2	Verapamil	Atenolol
LogP*		2.03	−0.21	−0.33
LogD*		2.03	1.87	−1.77
Mouse liver microsomes	%Metabolism in 30 min	94.5	80.0	
	Half-life (min)	6.0	11.0	
	CL_{int} (μL/min/mg protein)	243.5	130.0	
Rat liver microsomes	%Metabolism in 30 min	100.0	79.0	
	Half-life (min)	4.0	11.0	
	CL_{int} (μL/min/mg protein)	334.5	121.0	
Dog liver microsomes	%Metabolism in 30 min	58.5	81.0	
	Half-life (min)	18.5	11.0	
	CL_{int} (μL/min/mg protein)	77.5	131.0	
Human liver microsomes	%Metabolism in 30 min	100.0	79.0	
	Half-life (min)	0.0	11.0	
	CL_{int} (μL/min/mg protein)	143740	129.0	

* Partitioned towards n-octanol (lipophilic).

cycle at S and G2/M phase. Lastly, the structural similarity with soluble guanylate cyclase inhibitor LY83583. Based on these facts, we selected targets in cell cycle check-point control, i.e., ATR/CHK1 (S and G2/M), WEE1/CDK1 (G2/M), WEE1/CDK2 (S)[60] and soluble guanylate cyclase. Table 7 summarizes the estimated free energy of binding of **AQQ1-5** against the six selected target proteins. Since binding free energy is good for all the targets, we inspected the interaction profile of **AQQ2** with target proteins and compared it with the co-crystallized ligands of a respective target protein. Maximum overlapping interactions were considered for judging the probable drug targets. Accordingly, ATR, WEE1, and sGC were found to be probable targets for this series of compounds (Figure 7–9).

Figure 7 shows 2D-interaction plot for **AQQ2** and co-crystallized ligand 8DV with ATR (PDB: 5UK8). With the following residues both the ligands displayed hydrophobic interactions: MET800, LYS802, ASP810, TYR836, ILE848, GLU849, TRP850, VAL851, SER854, MET922, ILE932, and ASP933. A common H-bonding interaction was also been identified with backbone NH of VAL851. Similarly, Figure 8 captured the common hydrophobic and H-bonding interaction between **AQQ2** and respective co-crystallized ligand 8X7 with WEE1 protein (PDB: 5 V5Y). Common H-bonding interactions were found between the ligands and CYS379 residues of WEE1, additionally $-CF_3$ group of **AQQ2** established H-bonding interaction with ASP463. It is interesting to note that the fluorine of $-CF_3$ group establishes the crucial H-bonding interaction with both ATR and WEE1. In the case of sGC, Figure 9, **AQQ2** occupied the space where the highly hydrophilic sugar phosphate ester of GTP (substrate) lies. Quinone carbonyl oxygen and sidechain amino nitrogen of **AQQ2** were able to interact with catalytic Mg, similar to GTP's first phosphate ester oxygen. While another carbonyl oxygen displayed H-bonding interaction with PHE490, THR491, and GLY489 mimicking the interaction of the second and third phosphate groups of GTP. Based on these *in silico* investigations, we suppose that ATR, WEE1, and sGC may be the putative target for this series of compounds. Additional *in vitro* investigations are required for substantiating the claims based on *in silico* investigations presented here.

Table 7. Molecular docking simulation of **AQQ1-5** with ATR, CHK1, WEE1, CDK1 & CDK2.

Code	Estimated free energy of binding (kcal/mol)					
	ATR	CHK1	WEE1	CDK1	CDK2	sGC
	PDB: 5UK8	PDB: 6FC8	PDB: 5V5Y	PDB: 2YCQ	PDB: 6GUB	PDB: 6JT2
AQQ1	−7.16	−7.68	−8.82	−6.97	−7.59	−7.72
AQQ2	−7.32	−7.40	−7.92	−7.61	−7.94	−7.76
AQQ3	−7.40	−9.01	−7.52	−8.01	−7.87	−7.85
AQQ4	−7.54	−9.13	−8.08	−8.17	−8.87	−7.94
AQQ5	−7.13	−7.42	−7.3	−7.15	−7.55	−8.08

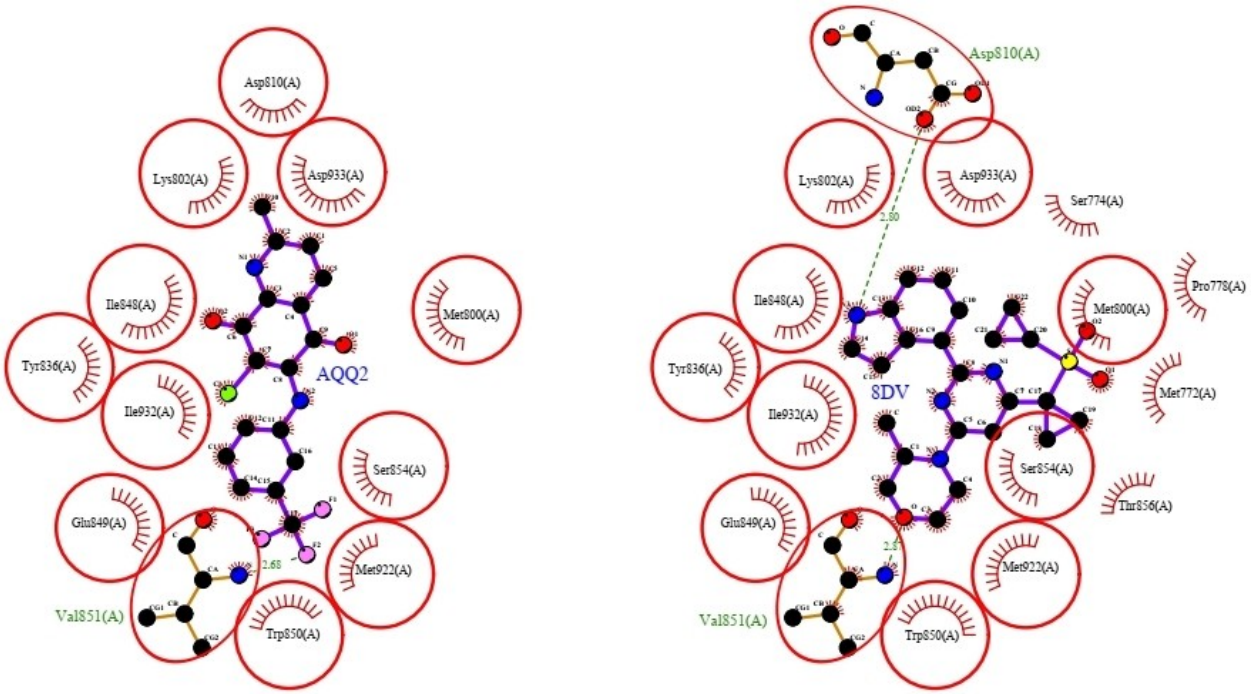

Figure 7. 2D-interaction plot of **AQQ2** & **8DV** (co-crystallized ligand) with ATR (PDB: 5UK8). Interacting residues common for both the ligands were shown in red circles, arc with red spikes indicates hydrophobic interaction, and dashed green line indicates H-bonding interaction. Atoms of amino acid residue and ligand are colored by atom type (Carbon: black, oxygen: red, nitrogen: blue, chlorine: green, fluorine: pink and sulphur: yellow), bonds of amino acid residues are colored brown, and ligands are colored violet.

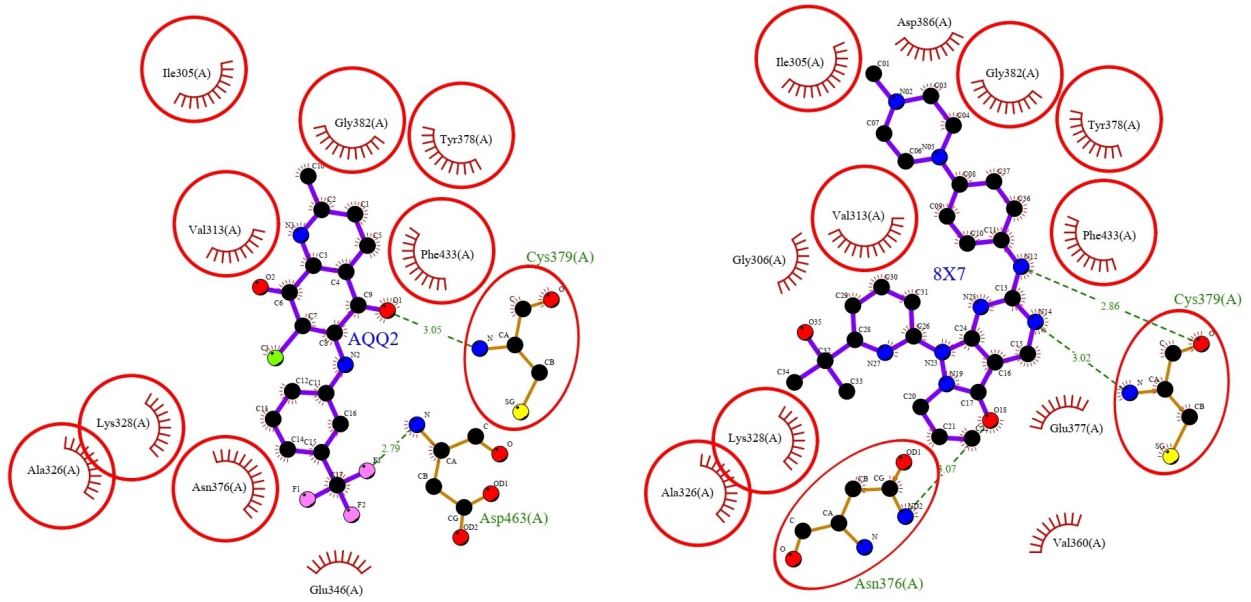

Figure 8. 2D-interaction plot of **AQQ2** & **8X7** (co-crystallized ligand) with WEE1 (PDB: 5 V5Y). Interacting residues common for both the ligands were shown in red circles, arc with red spikes indicates hydrophobic interaction, and dashed green line indicates H-bonding interaction. Atoms of amino acid residue and ligand are colored by atom type (Carbon: black, oxygen: red, nitrogen: blue, chlorine: green, fluorine: pink and sulfur: yellow), bonds of amino acid residues are colored brown, and ligands are colored violet.

4. Conclusions

Enthused by the biological significance of the aminated quinolinequinones, particularly with therapeutic potential, five aminated quinolinequinones (**AQQ1-5**) with electron-withdrawing group(s) (–CF_3 and –CN) at various positions of aryl amino ring were submitted and then firstly screened against the full NCI 60-cell lines panel at 10 μM concentration. Four of the five aminated quinolinequinones were the most potent of the AQQs and were selected by NCI screening at five doses. An agent

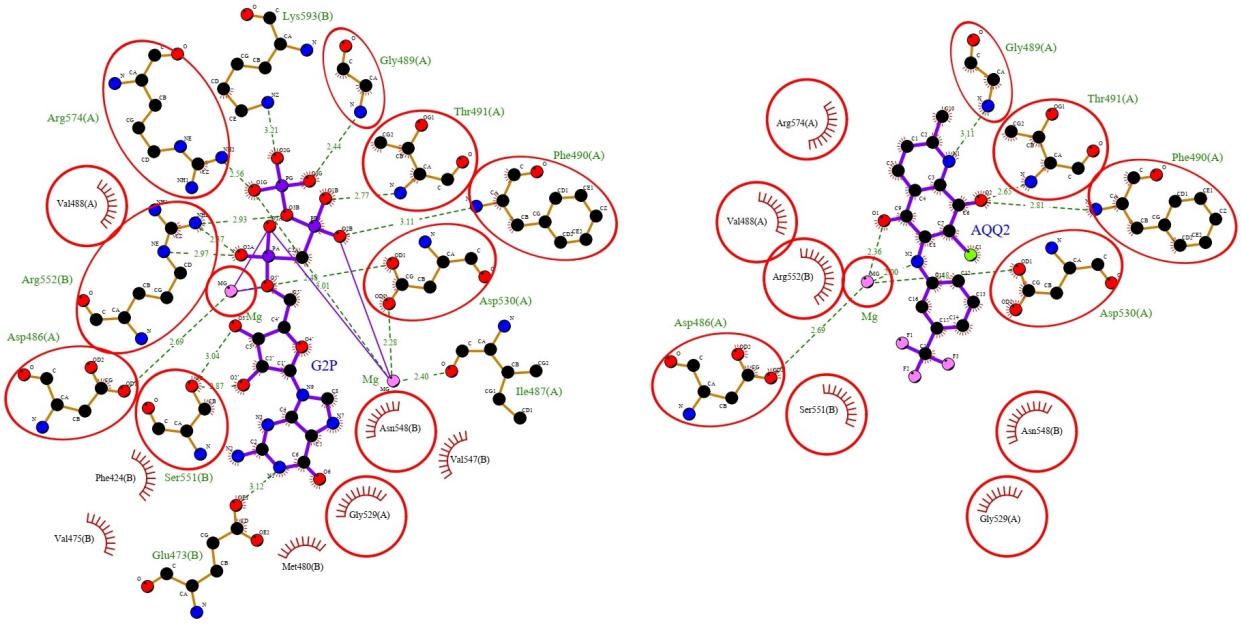

Figure 9. 2D-interaction plot of **G2P** (co-crystallized ligand) & **AQQ2** with sGC (PDB: 6JT2). Interacting residues common for both the ligands were shown in red circles, arc with red spikes indicates hydrophobic interaction, and dashed green line indicates H-bonding interaction. Atoms of amino acid residue and ligand are colored by atom type (Carbon: black, oxygen: red, nitrogen: blue, chlorine: green, and fluorine & Magnesium: pink), bonds of amino acid residues are colored brown, ligands are colored violet, and coordinate bonds are colored violet.

with a GI_{50} value of less than 2 μM is regarded as potent and may reflect selectivity towards that particular cancer cell lines for the purposes of analyzing the activity of quinolinequinones. Thus, all AQQs showed a super anticancer profile with low micromolar GI_{50} and TGI values against all leukemia cell lines (with the exception of RPMI-8226 cell lines for **AQQ4**), some non-small cell lung and ovarian cancer, most colon cancer, most melanoma and renal cancer, and some breast cancer cell lines. Additionally, using *in vitro* experiments, we showed that among the cell lines tested MCF7 and T-47D of breast cancer, DU-145 of prostate cancer, HCT-116 of colon cancer, and HaCaT human keratinocytes. MCF7 breast cancer was the most susceptible to **AQQ2**. Further, **AQQ2** induced apoptosis in MCF7 cells and caused alterations in the cell cycle. In addition, high concentrations of **AQQ2** increased intracellular ROS in MCF7 cells.

Acknowledgements

The authors present their thanks to the National Cancer Institute (NCI), Bethesda, Maryland, USA for carrying out the antiproliferative activity by the Developmental Therapeutics Program (DTP), Division of Cancer Treatment and Diagnosis, National Cancer Institute (http://dtp.cancer.gov).

Conflict of Interests

The authors declare no conflict of interest.

Data Availability Statement

The data that support the findings of this study are available from the corresponding author upon reasonable request.

Keywords: breast cancer · cytotoxicity · ADME · molecular docking

[1] G. M. Cooper, R. Hausman, *A molecular approach, The Cell. 2nd ed.* Sunderland, MA: Sinauer Associates, **2000**.
[2] L. Brannon-Peppas, J. O. Blanchette, *Adv. Drug Delivery Rev.* **2004**, *56(11)*, 1649–1659.
[3] A. Hebar, P. Valent, E. Selzer, *Expert Rev. Clin. Pharmacol.* **2013**, *6(1)*, 23–34.
[4] D. A. Gewirtz, M. L. Bristol, J. C. Yalowich, *Curr. Opin. Investig. Drugs* **2010** (London, England: 2000), *11(6)*, 612–614.
[5] N. A. Meanwell, *Chem. Res. Toxicol.* **2011**, *24(9)*, 1420–1456.
[6] R. Guha, in *On Exploring Structure–Activity Relationships*, (Ed. S. Kortagere), Humana Press, Totowa, NJ, **2013**, pp. 81–94.
[7] J.-C. Lien, L.-J. Huang, C.-M. Teng, J.-P. Wang, S.-C. Kuo, *Chem. Pharm. Bull.* **2021**, *69*, 661.
[8] J. Campanini-Salinas, J. Andrades-Lagos, N. Hinojosa, F. Moreno, P. Alarcón, G. González-Rocha, I. E. Burbulis, D. Vásquez-Velásquez, *Antibiotics* **2021**, *10(6)*, 614.
[9] L. P. Borba-Santos, C. D. Nicoletti, T. Vila, P. G. Ferreira, C. F. Araújo-Lima, B. V. D. Galvão, I. Felzenszwalb, W. de Souza, F. de Carvalho da Silva, V. F. Ferreira, *Braz. J. Microbiol.* **2022**, *53(2)*, 749–758.
[10] M. Janeczko, K. Kubiński, A. Martyna, A. Muzyczka, A. Boguszewska-Czubara, S. Czernik, M. Tokarska-Rodak, M. Chwedczuk, O. M. Demchuk, H. Golczyk, *J. Med. Microbiol.* **2018**, *67(4)*, 598–609.
[11] P. D. de Almeida, G. d. S. B. Jobim, C. C. dos Santos Ferreira, L. R. Bernardes, R. B. Dias, C. B. S. Sales, L. d. F. Valverde, C. A. Rocha, M. B. Soares, D. P. Bezerra, *Chem.-Biol. Interact.* **2021**, *343*, 109444.
[12] P. Mahalapbutr, R. Leechaisit, A. Thongnum, D. Todsaporn, V. Prachayasittikul, T. Rungrotmongkol, S. Prachayasittikul, S. Ruchirawat, V. Prachayasittikul, R. Pingaew, *CS Omega* **2022**, *7(21)*, 17881–17893.

[13] A. Alfadhli, A. Mack, L. Harper, S. Berk, C. Ritchie, E. Barklis, *Bioorg. Med. Chem.* **2016**, *24(21)*, 5618–5625.
[14] R. Pingaew, V. Prachayasittikul, A. Worachartcheewan, C. Nantasenamat, S. Prachayasittikul, S. Ruchirawat, V. Prachayasittikul, *Eur. J. Med. Chem.* **2015**, *103*, 446–459.
[15] P. F. Carneiro, M. C. Pinto, R. K. Marra, F. d. C. da Silva, J. A. Resende, L. F. R. e Silva, H. G. Alves, G. S. Barbosa, M. C. de Vasconcellos, E. S. Lima, *Eur. J. Med. Chem.* **2015**, *108*, 134–140.
[16] D.-Y Yuk, H. Y. Lee, C. K. Ryu, J. T. Hong, W. S. Kang, H. S. Yoo, Y. P. Yun, *Arzneimittel-Forschung-Drug Research* **2000**, *50(3)*, 254–259.
[17] J.-C. Lien, L.-J. Huang, C.-M. Teng, J.-P. Wang, S.-C. Kuo, *Chem. Pharm. Bull.* **2002**, *50(5)*, 672–674.
[18] C. Erasmus, J. Aucamp, F. J. Smit, R. Seldon, A. Jordaan, D. F. Warner, D. D. David, *Bioorg. Chem.* **2021**, *114*, 105118.
[19] V. K. Tandon, D. B. Yadav, A. K. Chaturvedi, P. K. Shukla, *Bioorg. Med. Chem. Lett.* **2004**, *15(13)*, 3288–3291.
[20] Y.-R. Jin, C.-K. Ryu, C.-K. Moon, M.-R. Cho, Y.-P. Yun, *Pharmacology* **2004**, *70(4)*, 195–200.
[21] D.-Y. Yuk, C.-K. Ryu, J.-T. Hong, K.-H. Chung, W.-S. Kang, Y. Kim, H.-S. Yoo, M.-K. Lee, C.-K. Lee, Y.-P. Yun, *Biochem. Pharmacol.* **2000**, *60(7)*, 1001–1008.
[22] A. Richwien, G. Wurm, *Die Pharmazie* **2004**, *59(3)*, 163–169.
[23] E. C. Cerqueira, P. A. Netz, C. Diniz, V. P. do Canto, C. Follmer, *Bioorg. Med. Chem.* **2011**, *19(24)*, 7416–7424.
[24] N. El-Najjar, H. Gali-Muhtasib, R. A. Ketola, P. Vuorela, A. Urtti, H. Vuorela, *Phytochem. Rev.* **2011**, *10*, 353–370.
[25] C. Asche, *Mini-Rev. Med. Chem.* **2005**, *5(5)*, 449–467.
[26] T. Meier, G. Buyse, *J. Neurol.* **2009**, *256*, 25–30.
[27] L.-O. Klotz, X. Hou, C. Jacob, *Molecules* **2014**, *19(9)*, 14902–14918.
[28] T. J. Donohoe, C. R. Jones, L. C. Barbosa, *J. Am. Chem. Soc.* **2011**, *133(41)*, 16418–16421.
[29] A. D. Bolzán, M. S. Bianchi, *Mutat. Res. Rev. Mutat. Res.* **2001**, *488(1)*, 25–37.
[30] A. J. Primeau, A. Rendon, D. Hedley, L. Lilge, I. F. Tannock, *Clin. Cancer Res.* **2005**, *11(24)*, 8782–8788.
[31] H. Taymaz-Nikerel, M. E. Karabekmez, S. Eraslan, B. Kırdar, *Sci. Rep.* **2018**, *8(1)*, 13672.
[32] A. Im, A. Amjad, M. Agha, A. Raptis, J.-Z. Hou, R. Farah, S. Lim, A. Sehgal, K. A. Dorritie, R. L. Redner, *Oncol. Res.* **2016**, *24(2)*, 73.
[33] M. Cristofanilli, F. A. Holmes, L. Esparza, V. Valero, A. U. Buzdar, J. A. Neidhart, G. N. Hortobagyi, *Breast Cancer Res. and Treat.* **1999**, *54*, 225–233.
[34] M. A. Dahlem Junior, R. W. Nguema Edzang, A. L. Catto, J.-M. Raimundo, *Int. J. Mol. Sci.* **2022**, *23(22)*, 14108.
[35] K. W. Wellington, V. Hlatshwayo, N. I. Kolesnikova, S. T. Saha, M. Kaur, L. R. Motadi, *Invest. New Drugs* **2020**, *38*, 378–391.
[36] M. Kadela-Tomanek, E. Bębenek, E. Chrobak, M. Latocha, S. Boryczka, *Molecules* **2017**, *22(3)*, 447.
[37] M. Kadela, M. Jastrzębska, E. Bębenek, E. Chrobak, M. Latocha, J. Kusz, M. Książek, S. Boryczka, *Molecules* **2016**, *21(2)*, 156.
[38] H. Li, M. Cai, F. Cao, D. Yu, J. Yang, W. Yu, C. Chu, X. Guan, J.-J. Qin, J. Dong, *Bioorg. Med. Chem.* **2022**, *71*, 116941.
[39] A. Morris, R. Hoyle, P. P. Pagare, S. U. Zaman, Z. Ma, J. Li, Y. Zhang, *Bioorg. Chem.* **2022**, *124*, 105812.
[40] E. Mataracı-Kara, N. Bayrak, M. Yıldız, H. Yıldırım, A. F. TuYuN, *Antibiotics-Basel* **2022**, *11(10)*, 1397.
[41] H. Ciftci, B. Sever, N. Bayrak, M. Yıldız, H. Yıldırım, H. Tateishi, M. Otsuka, M. Fujita, A. F. Tuyun, *Pharmaceuticals* **2022**, *15(10)*, 1266.
[42] H. Yıldırım, M. Yıldız, N. Bayrak, E. Mataracı-Kara, B. Özbek-Çelik, M. Otsuka, M. Fujita, M. O. Radwan, A. F. Tuyun, *RSC Adv.* **2022**, *12(32)*, 20507–20518.
[43] H. Yıldırım, M. Yıldız, N. Bayrak, E. Mataracı-Kara, M. O. Radwan, A. T. Jannuzzi, M. Otsuka, M. Fujita, A. F. Tuyun, *Pharmaceuticals* **2022**, *15(5)*, 586.
[44] E. Mataracı-Kara, N. Bayrak, M. Yıldız, H. Yıldırım, B. Özbek-Çelik, A. F. Tuyun, *Drug Dev. Res.* **2022**, *83(3)*, 628–636.
[45] M. S. Ricci, W.-X. Zong, *Oncologist* **2006**, *11(4)*, 342–357.
[46] A. Razaghi, K. Heimann, P. M. Schaeffer, S. B. Gibson, *Apoptosis* **2018**, *23*, 93–112.
[47] M. R. Boyd, K. D. Pauli, *The NCI in vitro anticancer drug discovery screen. Anticancer Drug Development Guide*, Humana Press Totowa, NJ, **1997**, pp. 23–42.
[48] A. Monks, D. Scudiero, P. Skehan, R. Shoemaker, K. Paull, D. Vistica, C. Hose, J. Langley, P. Cronise, A. Vaigro-Wolff, *JNC* **1991**, *83(11)*, 757–766.
[49] M. R. Grever, S. A. Schepartz, B. A. Chabner, *Semin. Oncol.* **1992**, 622–638.
[50] H. Yildirim, N. Bayrak, M. Yildiz, F. N. Yilmaz, E. Mataraci-Kara, D. Shilkar, V. Jayaprakash and A. F. TuYuN, *Molecules* **2022**, *27*.
[51] N. Bayrak, H. Yıldırım, M. Yıldız, M. O. Radwan, M. Otsuka, M. Fujita, H. I. Ciftci, A. F. Tuyun, *Chem. Biol. Drug Des.* **2020**, *95(3)*, 343–354.
[52] N. Bayrak, H. Yıldırım, M. Yıldız, M. O. Radwan, M. Otsuka, M. Fujita, A. F. Tuyun, H. I. Ciftci, *Bioorg. Chem.* **2019**, *92*, 103255.
[53] H. I. Ciftci, N. Bayrak, H. Yıldırım, M. Yıldız, M. O. Radwan, M. Otsuka, M. Fujita, A. F. Tuyun, *Arch. Pharm.* **2019**, *352(12)*, 1900170.
[54] A. Fernandez, S. P. Laila, A. S. Nair, V. Vishnu, *J. Biomol. Struct. Dyn.* **2022**, *40(9)*, 3917–3927.
[55] N. Bayrak, H. I. Ciftci, M. Yıldız, H. Yıldırım, B. Sever, H. Tateishi, M. Otsuka, M. Fujita, A. F. Tuyun, *Chem.-Biol. Interact.* **2021**, *345*, 109555.
[56] Y. Ling, Q.-X. Yang, Y.-N. Teng, S. Chen, W.-J. Gao, J. Guo, P.-L. Hsu, Y. Liu, S. L. Morris-Natschke, C.-C. Hung, *Eur. J. Med. Chem.* **2018**, *154*, 199–209.
[57] C. Gorrini, I. S. Harris, T. W. Mak, *Nat. Rev. Drug Discovery* **2013**, *12(12)*, 931–947.
[58] Z. A. Stewart, M. D. Westfall, J. A. Pietenpol, *Trends Pharmacol. Sci.* **2003**, *24(3)*, 139–145.
[59] D. Lodygin, A. Menssen, H. Hermeking, *J. Clin. Invest.* **2002**, *110(11)*, 1717–1727.
[60] H. L. Smith, H. Southgate, D. A. Tweddle, *N. J. Expert Rev. Mol. Med.* **2020**, *22*, e2.

Manuscript received: June 11, 2023
Accepted manuscript online: August 17, 2023
Version of record online: ■■, ■■